CHINESE OPTICS LETTERS

Vol. 22, No. 4 | April 2024

Dynamic range expansion for optical frequency shift detection based on multiple harmonics

Yanru Zhou (周彦汝)[1,2*], Lifan Fan (樊李凡)[1,3], Kai Xu (徐 凯)[1,3], Wenyao Liu (刘文耀)[1,3], Enbo Xing (邢恩博)[1,3], Jun Tang (唐 军)[1,3], and Jun Liu (刘 俊)[1,3**]

[1] State Key Laboratory of Dynamic Measurement Technology, North University of China, Taiyuan 030051, China

[2] School of Information & Communication Engineering, North University of China, Taiyuan 030051, China

[3] School of Instrument & Electronics, North University of China, Taiyuan 030051, China

*Corresponding author: zhouyanru@nuc.edu.cn

**Corresponding author: liuj@nuc.edu.cn

Received November 20, 2023 | Accepted January 2, 2024 | Posted Online April 25, 2024

Sensors based on optical resonators often have their measurement range limited by their cavity linewidth, particularly in the measurement of time-varying signals. This paper introduces a method for optical frequency shift detection using multiple harmonics to expand the dynamic range of sensors based on optical resonators. The proposed method expands the measurement range of optical frequency shift beyond the cavity linewidth while maintaining measurement accuracy. The theoretical derivation of this method is carried out based on the equation of motion for an optical resonator and the recursive relationship of the Bessel function. Experimental results show that the dynamic range is expanded to 4 times greater than the conventional first harmonic method while still maintaining accuracy. Furthermore, we present an objective analysis of the correlation between the expansion factor of the method and the linewidth and free spectrum of the optical resonator.

Keywords: optical resonator; optical frequency shift; multiple harmonics; dynamic range expansion.

DOI: 10.3788/COL202422.041201

1. Introduction

Currently, sensors based on optical resonators are widely used for electrical[1,2], magnetic[3,4], and inertial[5–7] measurements. There are two sensing modes for this type of sensor: the first mode detects the average signal strength in a static way, while the second senses the dynamic signal in a dynamic way. The dynamic signal carries a time-dependent signal, while the dynamic mode detection process skillfully avoids low-frequency noise. This ability is advantageous for enhancing the signal-to-noise ratio of sensors based on optical resonators. This detection method has gained widespread adoption in various fields, including inertial sensing[8,9], electric[10] and magnetic intensity[11–13] measurement, and others. Sensors based on optical resonators have two crucial parameters: sensitivity and dynamic range. To enhance detection sensitivity, optical resonators with small linewidths are frequently employed. However, the nonlinear nature of the Lorentzian pattern within the resonant cavity curbs the measurement range. When the optical frequency shift goes beyond the optical resonator's linewidth[14–16], the output of the optical resonant cavity will show distortion, leading to nonlinear measurement outcomes. As a result, an optical resonator with a smaller linewidth enhances the detection precision but also considerably curtails the measurement scope of the sensor, which restricts the dynamic range.

The Pound–Drever–Hall (PDH) feedback control technique is commonly used in most experiments to increase the measurement range of the sensors based on optical resonators in static sensing[17–20]. This method locks the laser frequency to the resonant frequency of the optical resonator and uses the error signal of the feedback as the measurement result. This method can extend the measurement range limit of static sensing from the cavity linewidth to the tuning range of the laser. However, In dynamic sensing, traditional detection methods based on the first harmonic are still limited by the resonator linewidth[21,22]. Long *et al.* employed an optical frequency comb to detect the changes of the center frequency in the optical resonator. This approach extends the measurement range by approximately 110 times; however, the resolution is reduced by 33 times, resulting in a 3.5 times improvement in the dynamic range[23–25]. At the same time, this method requires a high-precision electro-optic phase modulator, additional complexity, and very complex data processing systems.

In this paper, we present a detection scheme for resonant frequency shifts in optical resonators that utilizes multiple harmonics. This method requires no additional equipment for the existing optical system and extracts frequency shift information from various harmonics present in the output signal of the optical resonator. Additionally, it has the ability to expand the measurement range of optical frequency shifts beyond the linewidth of the optical resonator, as shown in Fig. 1(b). The multiple harmonics method involves two parts: the first harmonic method and the first three harmonics method. The former is implemented when the optical frequency shift falls within the linewidth of the resonator, while the latter is utilized when it exceeds that linewidth. The feasibility of the first three harmonics method is theoretically demonstrated through comprehensive analysis. In the experiment, it has been verified that the application of the multiple harmonics method significantly extends the measurement range by 4 times compared to the traditional first harmonic method, while high measurement accuracy is maintained. In addition, this study investigates the maximum expansion factor of the multiple harmonics method. The limitation of the expansion factor is related to the free spectral range (FSR) of the optical resonator.

Theory: The equation of motion for an optical resonator is given by Eq. (1)[26],

$$\frac{\mathrm{d}a(t)}{\mathrm{d}t} = \left\{ i[\Delta - G(t)] - \frac{\Gamma_t}{2} \right\} a(t) + i\sqrt{\Gamma_{\mathrm{ex}}} A_{\mathrm{in}}, \tag{1}$$

where $a(t)$ is the amplitude of the optical field in the optical resonator[27], Δ represents the disparity between the resonant frequency of the optical resonator and the laser frequency, $G(t)$ denotes the sinusoidal dynamic input frequency shift of the optical resonator, and $G(t) = \Omega \sin(\omega_0 t)$, Ω is its amplitude and ω_0 is its frequency. Γ_t indicates the linewidth of the optical resonator, Γ_{ex} represents the amount of coupled additional loss coefficient, and A_{in} is the amplitude of the laser.

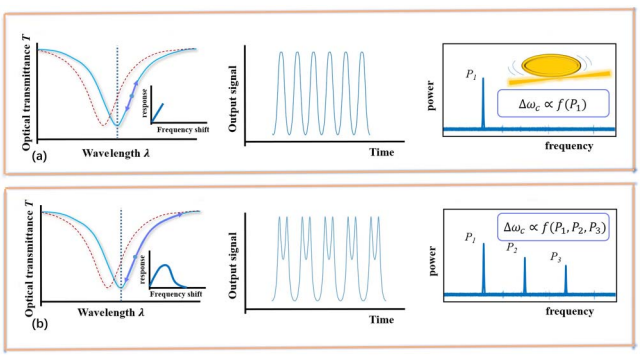

Fig. 1. (a) Output response of the optical resonator when the optical frequency changes within its linewidth; (b) output response of the optical resonator when the optical frequency changes beyond its linewidths.

By integrating Eq. (1), we have

$$a(t) = i\sqrt{\Gamma_{\mathrm{ex}}} A_{\mathrm{in}} \int_0^{\infty} \mathrm{d}\tau \exp\left[\left(i\Delta - \frac{\Gamma_t}{2} \right) \tau \right] \times \exp\left[-i \int_0^{\tau} \mathrm{d}\tau' G(t - \tau') \right]. \tag{2}$$

In the optical resonator, $\tau = \frac{2}{\Gamma_t}$. After integral of τ', there is

$$a(t) = i\sqrt{\Gamma_{\mathrm{ex}}} A_{\mathrm{in}} \int_0^{\infty} \mathrm{d}\tau \exp\left[\left(i\Delta - \frac{\Gamma_t}{2} \right) \tau \right] \exp\left[\frac{-2i}{\Gamma_t} G(t) \right]. \tag{3}$$

Substituting $G(t) = \Omega \sin(\omega_0 t)$ and integrating, we have

$$a(t) = \frac{-i\sqrt{\Gamma_{\mathrm{ex}}} A_{\mathrm{in}}}{i\Delta - \frac{\Gamma_t}{2}} \exp\left[\frac{-2i\Omega}{\Gamma_t} \sin(\omega_0 t) \right]. \tag{4}$$

In this case, the optical resonator is solely modulated by the incoming sinusoidal dynamic input frequency shift signal. The power transmitted by the cavity, $P(t)$, is

$$P(t) = |A_{\mathrm{in}} + i\sqrt{\Gamma_{\mathrm{ex}}} a(t)|^2. \tag{5}$$

Substituting Eq. (4) into Eq. (5),

$$P(t) = |A_{\mathrm{in}}|^2 \left| 1 + \frac{\Gamma_{\mathrm{ex}}}{\Delta^2 + \left(\frac{\Gamma_t}{2} \right)^2} \exp[-i(\Phi_0 + \Phi_m)] \right|^2, \tag{6}$$

where $\Phi_0 = \arctan(-\frac{\Delta}{\Gamma_t/2})$, $\Phi_m = \frac{2\Omega}{\Gamma_t} \sin(\omega_0 t)$.

$$P(t) = |A_{\mathrm{in}}|^2 \left\{ 1 + \left[\frac{\Gamma_{\mathrm{ex}}}{\Delta^2 + \left(\frac{\Gamma_t}{2} \right)^2} \right]^2 + \frac{2\Gamma_{\mathrm{ex}}}{\Delta^2 + \left(\frac{\Gamma_t}{2} \right)^2} \cos(\Phi_0 + \Phi_m) \right\}, \tag{7}$$

$$P(t) = P_{\mathrm{DC}} + \delta P(t), \tag{8}$$

where P_{DC} is the DC portion of the transmitted power and $\delta P(t)$ is the time-varying portion of the transmitted power,

$$\delta P(t) = \frac{2\Gamma_{\mathrm{ex}}}{\Delta^2 + \left(\frac{\Gamma_t}{2} \right)^2} [\cos(\Phi_0)\cos(\Phi_m) - \sin(\Phi_0)\sin(\Phi_m)]. \tag{9}$$

Utilizing the Bessel function,

$$\cos(\Phi_m) = \cos\left[\frac{2\Omega}{\Gamma_t} \sin(\omega_0 t) \right] = J_0\left(\frac{2\Omega}{\Gamma_t} \right) + 2\sum_{n=1}^{\infty} J_{2n}\left(\frac{2\Omega}{\Gamma_t} \right) \cos(2n\omega_0 t), \tag{10}$$

$$\sin(\Phi_m) = \sin\left[\frac{2\Omega}{\Gamma_t}\sin(\omega_0 t)\right] = 2\sum_{n=0}^{\infty} J_{2n+1}\left(\frac{2\Omega}{\Gamma_t}\right)\cos[(2n+1)\omega_0 t]. \quad (11)$$

Substituting Eqs. (10) and (11) into Eq. (9),

$$P(t) = \frac{2\Gamma_{ex}}{\Delta^2 + \left(\frac{\Gamma_t}{2}\right)^2}\left\{J_0\left(\frac{2\Omega}{\Gamma_t}\right)\cos(\Phi_0) + 2\sum_{n=1}^{\infty} J_{2n}\left(\frac{2\Omega}{\Gamma_t}\right)\cos(\Phi_0)\cos(2n\omega_0 t) - 2\sum_{n=0}^{\infty} J_{2n+1}\left(\frac{2\Omega}{\Gamma_t}\right)\sin(\Phi_0)\sin[(2n+1)\omega_0 t]\right\}. \quad (12)$$

The amplitudes of each harmonic order can be obtained from Eq. (12). According to the recursive relationship of the Bessel function,

$$2nJ_n(\eta) = \eta[J_{n+1}(\eta) + J_{n-1}(\eta)], \quad (13)$$

the relationship between the first three harmonics is derived as follows:

$$4\frac{P_2}{\cos(\Phi_0)} = -\frac{2\Omega}{\Gamma_t}\left(\frac{P_1 + P_3}{\sin(\Phi_0)}\right), \quad (14)$$

where P_1, P_2, and P_3 are the amplitudes of the first three harmonics of the output signal in the optical resonator, respectively. The resonance frequency shift Ω of the optical resonant cavity can be explicitly expressed through the subsequent formula,

$$\Omega = -2\Gamma_t \tan(\Phi_0)\frac{P_2}{P_1 + P_3}. \quad (15)$$

Substituting $\Phi_0 = \arctan(-\frac{\Delta}{\Gamma_t/2})$ into Eq. (15),

$$\Omega = 4\Delta\frac{P_2}{P_1 + P_3}. \quad (16)$$

In our experiments, we obtain the first three harmonics' amplitude of the output signal of the resonant cavity using Fourier transform. When the optical frequency shift input in the resonant cavity is within the measurement range of the first harmonic method, Ω is calculated using P_1. However, when the optical frequency shift input in the resonant cavity exceeds the measurement range of the first harmonic method, P_1, P_2, and P_3 are substituted into Eq. (16) to facilitate the calculation of Ω.

2. Experiment

An experimental system is constructed, as depicted in Fig. 2(a). The tunable laser with a narrow linewidth (RIO) emits 1550 nm light, which passes through the isolator and attenuator, and is

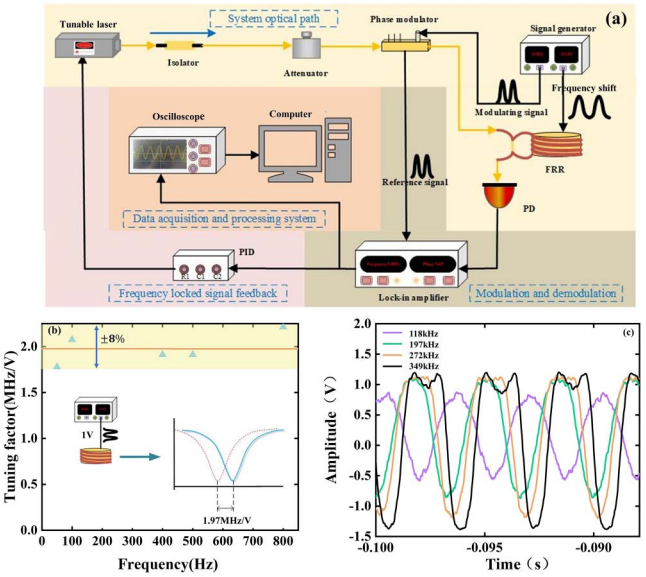

Fig. 2. (a) Experimental system of the multiple harmonics method; (b) tuning factor of PZT to the fiber resonant cavity; (c) output signals of the fiber resonant cavity after different optical frequency shift inputs.

modulated by the phase modulator with a sinusoidal signal. The light then enters the fiber ring resonator (FRR). The output light signal of the FRR is detected by a photodetector, which converts the light signal to an electrical signal. This electrical signal is demodulated and sideband frequency-locked using a phase-locked amplifier and a proportional-integral-derivative (PID) controller, where the error signal of the sideband locking is fed back into the laser through a feedback loop. The output signal of the FRR is acquired using an oscilloscope, and the data are processed in the computer. The FRR utilizes a 99:1 coupler and is wrapped on PZT for easy control of the optical frequency shift input. The linewidth of the FRR is 560 kHz, with a quality factor Q of 3.45×10^8. To ensure that the locking position of the first-order sideband frequency lies within the linewidth of the FRR, the sinusoidal modulation frequency is set to 101 kHz. One sideband is locked to the cavity at the maximum slope point on the side of the optical resonance, which enhances the sensitivity of the sensors. Side-locking is achieved with a low bandwidth PID controller (≈200 Hz).

We calibrate the tuning factor of the PZT to optical frequency shift and evaluate the influence of the sinusoidal signal frequency on those tuning factors, as shown in Fig. 2(b). We apply a sinusoidal signal with an amplitude of 1 V and frequencies ranging from 50 to 800 Hz to the PZT. Experimental results show that the frequency of this sinusoidal signal has little impact on the tuning factor. The mean value of the tuning factor is 1.97 MHz/V. Since the PDH frequency-locked loop has a bandwidth of 200 Hz, we use a sinusoidal signal with a frequency of 300 Hz for the PZT in our experiment. By adjusting the amplitude of this sinusoidal signal applied to the PZT, we dynamically change the frequency shift input of the FRR. Figure 2(c) displays the FRR output signal. When the amplitudes of the optical frequency shift are 118 and 197 kHz, which fall within the

linewidth of the resonant cavity, the output signal remains distortion-free. There exists a direct proportional relationship between the amplitude of the first harmonic component of the output signal and the optical frequency shift. However, when the optical frequency shifts are 272 and 349 kHz, which surpass the linewidth, distortion is generated at the output signal. As a result of this distortion, there is no longer a linear relationship between the optical frequency shift and the amplitude of the first harmonic component of the output signal. Therefore, it is not suitable to use only the first harmonic method for calculating optical frequency shift in this scenario. According to Eq. (16), for detecting and calculating the optical frequency shift, the first three harmonics should be utilized. To acquire the amplitude of the first three harmonics of the output signal, the output signal of the FRR is Fourier-transformed, and then the amplitude is used to determine the optical frequency shift according to Eq. (16).

The experiment demonstrates that the linear range of the first harmonic method spans from 0 to 197 kHz, which aligns with theoretical predictions based on the linewidth of the resonant cavity and the locking point at the first-order sideband. The optical frequency shift is normalized to the linear measurement range of the first harmonic method ($\Omega/\Omega_{(1)}$, that is, $\Omega/197$ kHz). As shown in Fig. 3(a), with increasing optical frequency shift, there is a gradual increase in the amplitude of the first harmonic first. Then there is a deceleration in its growth rate. Finally, there is a gradual decrease. Figures 3(b)–3(e) demonstrate that when the input optical frequency shift is much lower than the linewidth of the FRR, the amplitude of the first harmonic increases linearly with the frequency shift. Additionally, the amplitude of the first harmonic is significantly greater than that of the second and third harmonics. The latter two are negligible in comparison to the first harmonic. When the input optical frequency shift exceeds the linear range of the first harmonic method, the amplitude of the first harmonic cannot increase linearly with the increase of frequency shift, whereas the amplitudes of the second and third harmonics increase rapidly. Energy is transferred to higher harmonics with the increase of the optical frequency shift.

The results calculated by the multiple harmonics method are shown in Fig. 4. Due to the limitations of the PDH frequency-locking loop, the optical frequency shift range is between 0 and 800 kHz. Figure 4(a) indicates that the first harmonic method can linearly measure the optical frequency shift with a linearity of 0.9964 when the frequency shift remains below 197 kHz. Above 197 kHz, the error gradually increases between the measurement results and the input frequency shift. This experimental observation is consistent with the theoretical analysis. Figure 4(b) shows that when the optical frequency shift is between 197 and 800 kHz and the multiple harmonic method is implemented, the frequency shift calculated by the first three harmonics method aligns with the input frequency shift of the FRR. The linearity is 0.9942. This study demonstrates that the multiple harmonic method can significantly expand the measurement range of optical frequency shift. By extending the measurement range to 4 times that of the first harmonic method, we have validated the effectiveness of the multiple harmonics method in expanding the measurement range.

During the experiment, the resolution of the first harmonic method and multiple harmonics method is assessed in their respective test ranges. The input optical frequency shift is controlled at 1, 2, 3, 4, 5, and 6 kHz. Seven to ten sets of data points are tested at each frequency interval. In these sets of experiments, the experimental results are nonlinear when the test interval is less than 4 kHz, indicating that the first harmonic method and the multiple harmonics method are unable to detect

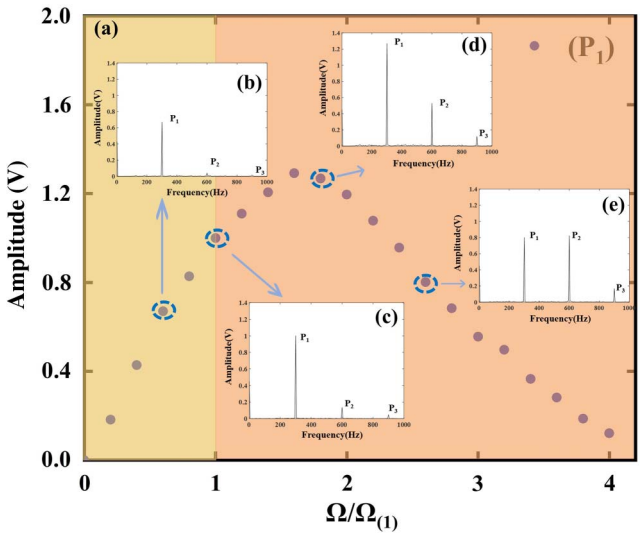

Fig. 3. (a) Variation of the first harmonic amplitude with gradually increasing optical frequency shift input, where $\Omega_{(1)}$ = 197 kHz; amplitude of the first three harmonics after Fourier transform of the output signals with optical frequency shift of (b) 118 kHz; (c) 198 kHz; (d) 354 kHz; (e) 512 kHz.

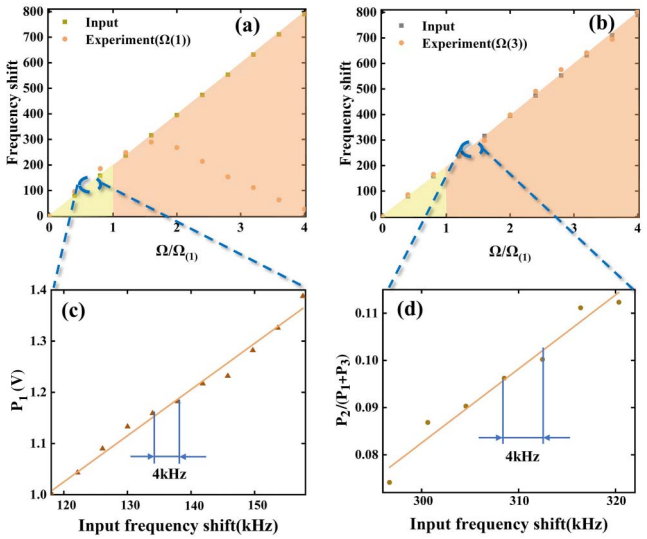

Fig. 4. (a) Experimental result of the first harmonic method; (b) experimental result of the multiple harmonics method; (c) resolution test of the first harmonic method in its linear range; (d) resolution test of the multiple harmonics method in its linear range.

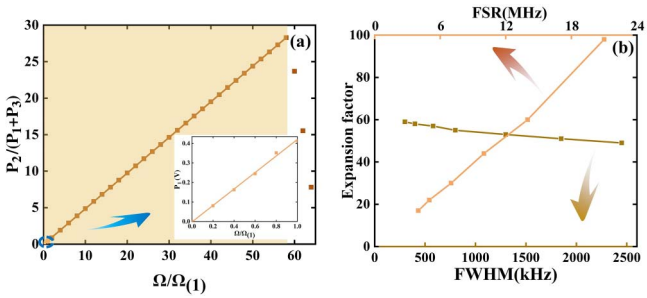

Fig. 5. (a) Theoretical limitation of dynamic range expansion with the FRR in our experiment; the inset of the figure shows the measurement range of the first harmonic method. (b) The expansion factor varies with the linewidth when the FSR is fixed; the expansion factor varies with the FSR when the linewidth is fixed.

optical frequency shifts up to 4 kHz. However, when the test interval is greater than or equal to 4 kHz, the experimental results are linear, indicating that the first harmonic method and the multiple harmonics method can effectively discriminate optical frequency shifts greater than or equal to 4 kHz. As can be seen in Figs. 4(c) and 4(d), both the first harmonic method and multiple harmonics method have a minimum resolution of 4 kHz. This confirms that the multiple harmonics method expands the range of measurements while maintaining accuracy. The goal of broadening the dynamic range for measurement of the input optical frequency shift is accomplished.

3. Limits of the Multiple Harmonics Method

In our experiments, we expand the dynamic range to four times by multiple harmonics method compared with the first harmonic method. However, this is not the limit of the multiple harmonics method. The experimental result of four times is limited by the feedback circuit of the experimental system. In our experimental system, when the optical frequency shift is excessive, PDH sideband locking for the FRR will be disabled, and the output signal of the optical resonator cannot be obtained. Therefore, we investigate the limitations of the multiple harmonics method and its potential to increase dynamic range in theory.

In this study, we introduce the concept of the expansion factor, which is defined as the ratio between the linear measurement range of the multiple harmonics method and the linear measurement range of the first harmonic method. As show in Fig. 5(a), for a 15-m fiber-resonant cavity in our experiment, the theoretical expansion factor is 58, greatly exceeding the linewidth of the resonant cavity. Meanwhile, the effect of linewidth and FSR on the expansion factor of the multiple harmonics method is analyzed. The results demonstrate that the linewidth variation has a small impact on the expansion factor when the FSR is fixed. Then we investigated the impact of FSR on the expansion factor of the multiple harmonics method by fixing its intracavity loss and varying the length of FRR. The result indicates that the FSR has a significant impact on the expansion factor. When the linewidth is fixed, a larger FSR means a larger expansion factor. This provides a reference for the selection on the parameters of the optical resonator according to the requirements of the expansion factor.

4. Conclusion

In this paper, we propose and assess the technique for expanding the dynamic range of optical frequency shift detection that relies on multiple harmonics. Our analysis combines theoretical and experimental approaches. We integral and calculate the equations of motion for the optical field within the resonant cavity. Then the equations of the time-varying optical power are obtained. This confirms the feasibility of the multiple harmonics method in theory. Experimental results show that the multiple harmonics method expands the measurement range of the optical frequency shift beyond its linewidth, with an expansion factor of four times compared with the first harmonic method. Moreover, the multiple harmonics method maintains measurement accuracy of 4 kHz, which is equivalent to that of the first harmonic method. The theoretical limits of the multiple harmonics method have been studied. It is found that expansion factor is closely related to the FSR of the optical resonator. An optical resonator with a large FSR can realize a large expansion factor. Without introducing any optical devices, the multiple harmonics method is demonstrated as a simple and cost-effective approach that provides high measurement accuracy and large measurement range for the dynamic signals at the same time.

Acknowledgements

This work was supported by the National Natural Science Foundation of China (NSFC) (No. 52305621), Foundation Research Project of Shanxi Province (No. 202203021212156), and Shanxi Province Key Laboratory of Quantum Sensing and Precision Measurement (No. 201905D121001002).

References

1. M. Luo, Q. Yang, F. Dong, *et al.*, "Miniature micro-ring resonator sensor with electro-optic polymer cladding for wide-band electric field measurement," J. Light. Technol. **40**, 2577 (2022).
2. D. N. Roxby, Z. Yuan, S. Krishnamoorthy, *et al.*, "Enhanced biophotocurrent generation in living photosynthetic optical resonator," Adv. Sci. **7**, 1903707 (2020).
3. R. Gao, D. F. Lu, J. Cheng, *et al.*, "Temperature-compensated fibre optic magnetic field sensor based on a self-referenced anti-resonant reflecting optical waveguide," Appl. Phys. Lett. **110**, 131903 (2017).
4. S. Pu, L. Mao, T. Yao, *et al.*, "Microfiber coupling structures for magnetic field sensing with enhanced sensitivity," IEEE Sens. J. **17**, 5857 (2017).
5. Y. Zhang, Z. Wang, G. Wang, *et al.*, "Polarization stability of spun fiber resonator for resonant fiber optic gyro," IEEE Sens. J. **23**, 15644 (2023).
6. L. Feng, X. Ren, X. Deng, *et al.*, "Analysis of a hollow core photonic bandgap fiber ring resonator based on micro-optical structure," Opt. Express **20**, 18202 (2012).
7. Z. Wang, G. Wang, S. Kumar, *et al.*, "Recent advancements in resonant fiber optic gyro—a review," IEEE Sens. J. **22**, 18240 (2022).

8. S. Bramhavar, D. Kharas, and P. W. Juodawlkis, "A photonic integrated resonant accelerometer," in *IEEE Photonics Conference (IPC)* (2016), p. 1.
9. Y. Huang, J. G. Flor Flores, Y. Li, *et al.*, "A chip-scale oscillation-mode optomechanical inertial sensor near the thermodynamical limits," Laser Photonics Rev. **14**, 1800329 (2020).
10. A. A. Savchenkov, W. Liang, V. S. Ilchenko, *et al.*, "Photonic E-field sensor," AIP Adv. **4**, 122901 (2014).
11. S. Forstner, S. Prams, J. Knittel, *et al.*, "Cavity optomechanical magnetometer," Phys. Rev. Lett. **108**, 120801 (2012).
12. S. Forstner, E. Sheridan, J. Knittel, *et al.*, "Ultrasensitive optomechanical magnetometry," Adv. Mater. **26**, 6348 (2014).
13. B.-B. Li, G. Brawley, H. Greenall, *et al.*, "Ultrabroadband and sensitive cavity optomechanical magnetometry," Photonics Res. **8**, 1064 (2020).
14. J. Rong, W. Xu, E. Xing, *et al.*, "A high-sensitivity magnetic field sensor based on PDMS flexible resonator," Appl. Sci. **13**, 6274 (2023).
15. P. Zhou, K. Liang, Y. Wang, *et al.*, "Research on A high-sensitivity temperature sensor with multi-indicator based on nano-cylinder-loaded ring resonator," Photonics **10**, 69 (2023).
16. Q. Wang, X. Feng, Y. Zhao, *et al.*, "Fiber ring resonator based slow-light and high sensitivity gas sensing technology," Sens. Actuators B **214**, 197 (2015).
17. H. Li, J. Xu, X. Wang, *et al.*, "High-bandwidth tracking method of resonant frequency for sensing resonators," J. Light. Technol. **38**, 898 (2020).
18. C. Saavedra, D. Pandey, W. Alt, *et al.*, "Spectroscopic gas sensor based on a fiber Fabry-Perot cavity," Phys. Rev. Appl. **18**, 044039 (2022).
19. O. Arcizet, P. F. Cohadon, T. Briant, *et al.*, "High-sensitivity optical monitoring of a micromechanical resonator with a quantum-limited optomechanical sensor," Phys. Rev. Lett. **97**, 133601 (2006).
20. Y. G. Zhang, H. Li, N. Liu, *et al.*, "Design of real-time free spectral range measurement based on HOPLL technique," IEEE Sens. J. **20**, 10607 (2020).
21. Q. Liu, Z. He, and T. Tokunaga, "Sensing the earth crustal deformation with nano-strain resolution fiber-optic sensors," Opt. Express **23**, A428 (2015).
22. J. Chen, Q. Liu, X. Fan, *et al.*, "Ultrahigh resolution optical fiber strain sensor using dual Pound–Drever–Hall feedback loops," Opt. Lett. **41**, 1066 (2016).
23. D. A. Long, B. J. Reschovsky, F. Zhou, *et al.*, "Electro-optic frequency combs for rapid interrogation in cavity optomechanics," Opt. Lett. **46**, 645 (2021).
24. B. J. Reschovsky, D. A. Long, F. Zhou, *et al.*, "Intrinsically accurate sensing with an optomechanical accelerometer," Opt. Express **30**, 19510 (2022).
25. D. A. Long, B. J. Reschovsky, T. W. LeBrun, *et al.*, "High dynamic range electro-optic dual-comb interrogation of optomechanical sensors," Opt. Lett. **47**, 4323 (2022).
26. U. A. Javid, S. D. Rogers, A. Graf, *et al.*, "Cavity optomechanical sensing in the nonlinear saturation limit," Laser Photonics Rev. **10**, 1002 (2021).
27. M. Aspelmeyer, T. J. Kippenberg, and F. Marquardt, "Cavity optomechanics," Rev. Mod. Phys. **86**, 1391 (2014).